J Mater Sci (2007) 42:3177–3189
DOI 10.1007/s10853-006-1357-0

Properties of bonded-polypropylene-bead foams: data and modelling

N. J. Mills · A. Gilchrist

Received: 16 December 2005 / Accepted: 28 February 2006 / Published online: 15 January 2007

Abstract Various mechanical properties (uniaxial compression, Poisson's ratio, indentation resistance) were measured for both expanded polypropylene (EPP) foam and bonded-polypropylene-bead foam. Finite Element Analysis, used on Body Centred Cubic (BCC) lattice models of uniform sized beads, predicted that the compressive response of EPP was hardly affected by the small volume fraction of inter-bead channels, whereas the bonded-bead foam with 25% porosity should have a near-linear compressive impact response. The foam lateral expansion on compression was predicted to be less than 3.5%, which was confirmed by experiment. Computational Fluid Dynamics was used to predict the air permeability of the models. An overlapping sphere model confirmed an earlier analysis, whereas a wet Kelvin foam model gave slightly lower permeabilities. The permeability increases with the square of the bead diameter and with the 2.6th power of the porosity.

Introduction

Expanded polystyrene (EPS) and expanded polypropylene (EPP) bead foams are widely used protective packaging materials. In the moulding process, superheated steam [1] causes touching foam beads to expand and develop fused flat faces at their interfaces. Although bead expansion can be sufficient to close the inter-bead channels, it is usual to leave the channels slightly open, since this greatly accelerates the cooling and solidification phase of the moulding cycle [2]. Consequently, the foams contain a small volume fraction of inter-bead channels. In the cooling stage of moulding, steam diffuses from the beads, and makes a rapid exit from the moulding via the connected inter-bead channels.

These foams are assumed to behave like homogeneous solids, with mechanical properties determined by their average density [3, 4]. Ibba and Avalle [5] compared the mechanical properties of EPP of a range of densities. By plotting graphs on logarithmic scales, they determined the exponents (1.65 for Young's modulus and 1.36 for initial collapse stress) in the power law relationships between these quantities and foam density. Zohdi [6] analysed the upper and lower bounds for the compaction of hyperelastic cohesive granules; although the analysis was stated to relate to EPP, EPP yields on compression. A review of polyolefin foams [7] mentions that their Young's modulus, as a function of the foam density, falls below the prediction of theories that assumed the cell faces are flat, and above that of a theory that assumed some cell faces are wrinkled. The post-yield compressive hardening was largely determined by the compression of the cell gas. Consequently, the effects of inter-bead channels on the mechanical properties of EPP, EPS and bonded-polypropylene-bead foams have not been analysed.

Brock (www.brock.com) produces a material consisting of PP foam beads bonded together with a polyurethane adhesive. These have much larger void volume fractions than conventional EPP, and water can be poured through blocks of the foam. However

N. J. Mills (✉) · A. Gilchrist
Department of Metallurgy and Materials, University of Birmingham, Birmingham B15 2TT, UK
e-mail: N.J.Mills@bham.ac.uk

the foam permeability has not been characterized, and it is not known whether the material could provide sufficient ventilation for a bicycle helmet. Modelling of airflow in open-cell polyurethane foams [8] showed that the air permeability was a strongly increasing function of both the cell diameter and the mean area of cell face holes. The airflow permeability was in the range 0.6×10^{-9} to 1.7×10^{-9} m^2 for these foams. However, their >95% porosity contrasts with the circa 25% porosity of the Brock foams. Models of close-packed or overlapping spheres [9, 10] have been proposed for fluidized beds of particles or permeable sandstone respectively; the analysis gives the relationship between permeability and material porosity.

Material characterisation

Materials

The materials investigated are listed in Table 1. The Brock foams contain polypropylene foam beads, adhesively bonded together under pressure [11], while the BASF foams are steam moulded. The Brock foams, of nominal 3.0 and 5.5 lb ft^{-3} density, had been cut into 25 mm thick slices from a larger block. Consequently, the upper and lower surfaces of the sheet contained some cut, and some uncut, bead boundaries.

Microstructure

Figure 1 shows optical micrographs of the Brock foam sheet surfaces. The PP beads are slightly ellipsoidal in shape, and in some locations the sectioned contact between two beads appears as a straight line. The black coating on the beads is less than 10 μm thick, and appears to be non-uniformly thick. The channels between beads vary in width, in different locations in the foam. In some areas beads do not touch, so channels have lateral dimensions approximately equal to a bead radius.

When the Brock foam structure was examined at higher magnification in an optical stereo microscope, the internal foam cell structure is seen (Fig. 2). A scanning electron microscope (SEM) was not used, since the vacuum causes complete cells to expand and the faces to become tight. The cell size varies from bead to bead. Some cell faces are wrinkled, while others appear to be flat. The bead packing differs from that of EPP, where bead expansion in the liquid state in the mould causes the inter-bead faces to become large, and the channels to become very narrow (Fig. 3).

Table 1 Polypropylene foams investigated

Manufacturer	Tradename	Nominal density (kg m^{-3})	Measured density (kg m^{-3})
Brock	FPP3.0	48	32–36
	FPP5.5	88	75–77
BASF	Neopolen 24	24	27–28
	Neopolen 43	43	41–43
	Neopolen 60	60	59–61

Image analysis and porosity measurement

Photographs of the foam top surface were traced, to outline the boundary of beads that are visible. It was difficult to detect the area of top surface that is not cut, because bead surfaces just below the cut often have a similar contrast to cut surfaces. A Leica Quantimet 500 image analyser was used to determine, for the section, the bead length (longest diameter over 32 ferets), bead breadth (smallest diameter) and roundness. Results from two sections were pooled; Table 2 shows that the FPP5.5 foam has a smaller bead length and breadth than the FPP3.0 foam. The mean of the mean length and breadth was used as the mean bead diameter for later calculations.

To estimate the volume fraction of air channel V_A, blocks of foam of known dimensions (hence known volume) were wrapped with thin adhesive parcel tape with the top surface left uncovered. They were then immersed in water for 5 min at a depth of 10 cm, the taped surfaces carefully dried and reweighed. The

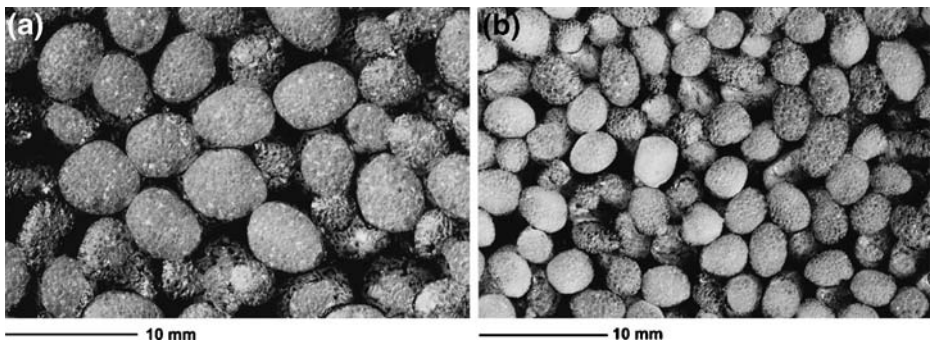

Fig. 1 Optical micrographs of Brock FPP foams showing sectioned beads (white) and inter-bead channels coated with a black adhesive layer: (a) density 34 kg m^{-3}, (b) 76 kg m^{-3}

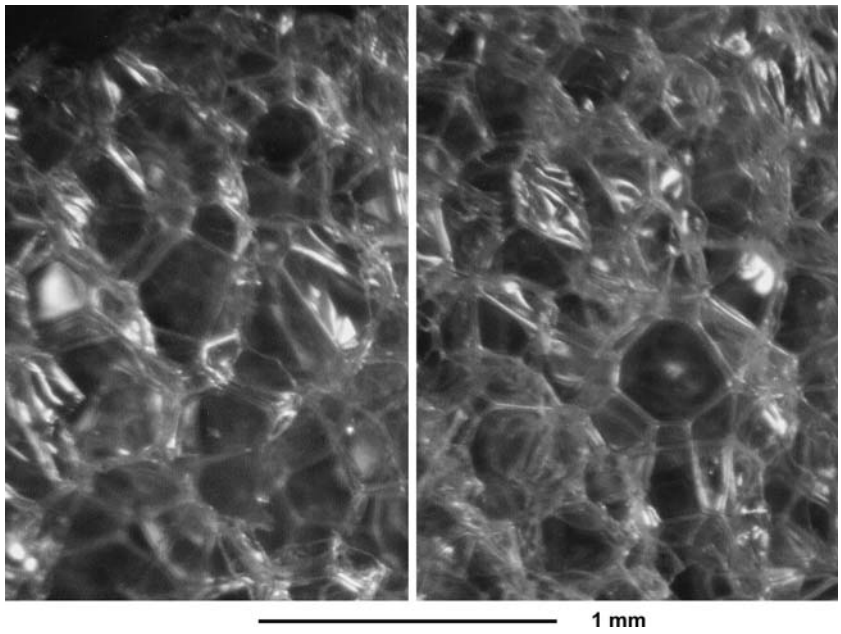

Fig. 2 Optical micrograph showing the foam cell structure of the Brock foams: left FPP3.0, right FPP5.5

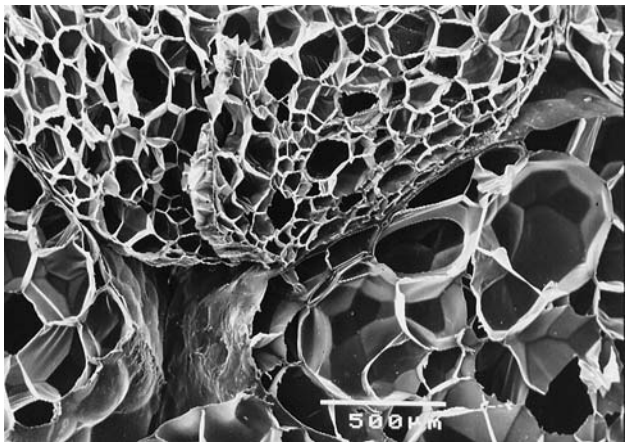

Fig. 3 SEM of BASF EPP of density 43 kg m^{-3} showing the cell structure, and sections of channels between four (base towards left) and three beads (top right)

Table 2 Characterization of bonded bead foams

Foam	Sample *n*	Bead length (mm)	Bead breadth (mm)	Bead round-ness	Volume fraction air
Brock FPP3.0	50	5.15 ± 0.88	4.01 ± 0.75	1.20 ± 0.15	0.24
Brock FPP5.5	95	3.52 ± 0.54	2.61 ± 0.35	1.13 ± 0.05	0.25

weight gain gives the volume of water that fills the channels, hence an estimate of $V_{A.}$ The real value could be slightly higher, as some narrow channels may not fill with water.

Property measurements

Several properties of bonded-bead foams may differ from those of conventional EPP bead foam. Consequently, the properties of the Brock foams were compared with those of BASF EPP foams of nominal densities 21 and 43 kg m^{-3}. These had been moulded into 150 by 500 by 1,500 mm blocks; a 10 mm layer, containing the denser skins of the blocks, was cut off prior to the preparation of test specimens with a band saw.

Compressive yield stress

The compressive yield responses, for two densities of Brock foams, were compared with those of BASF EPP foams. Specimens, 25 mm thick by 60 mm by 60 mm, were compression impact tested with an instrumented falling striker [12]. The drop height was 1.0 or 1.5 m, so the initial strain rate was between 177 and 217 s^{-1}. Integration of the striker acceleration allows the position of its lower surface to be computed as a function of time, hence the dynamic stress–strain curve to be determined. The compressive stress σ?versus engineering compressive strain ε data was fitted with the expression

$$\sigma = \sigma_0 + \frac{p_0 \varepsilon}{1 - \varepsilon - R} \quad (1)$$

where p_0 is the effective gas pressure in the undeformed foam and σ_0 is a constant polymer contribution. This equation is based on the assumptions [13] that the gas in

the cells is isothermally compressed, and that the foam has a zero Poisson's ratio. The foam relative density R is calculated as the foam density divided by the 910 kg m^{-3} density of polypropylene. A straight line was fitted to the loading part of a graph of stress against $\varepsilon/(1-\varepsilon-R)$ (Fig. 4), for the strain parameter between 0.4 and the maximum value (or 5.0 if smaller). p_0 was evaluated from the slope, and the initial yield stress σ_0 from the stress axis intercept, of the line (Table 3). To obtain a linear plot for the Brock FPP5.5 foam, the foam density was set empirically at 20 kg m^{-3} rather than the actual 76 kg m^{-3}. The initial, nearly-linear, part of the stress–strain curve, representing the elastic region, continues to higher strains for the Brock foams than for the EPP. For the lower density foams, p_0 is close to atmospheric pressure (101 kPa) but it is larger for the higher density foams, as the polymeric structure contributes to the foam hardening. For this reason, p_0 is called the *effective gas pressure*, as the actual gas pressure in the cells is atmospheric.

Figure 5 shows the initial compressive yield stress as a function of foam density, comparing literature values for low strain rates with the values determined here using Eq. 1. Ibba and Avalle [5] seem to define the initial collapse stress as the start of the 'plateau' region at about 5% compressive strain. The foam initial yield stress at impact strain rates (Table 3) is two to three times that at low strain rates (Table 4), but the effective gas pressure is relatively unchanged. The large effect on the initial yield stress of increasing the strain rate by a factor of 15,000 is due to the polypropylene glass transition temperature (circa 0 °C) being close to the test temperature of 23 °C. For EPP over a density range from 29 to 137 kg m^{-3}, the yield stress increased with the 1.35th power of foam density [5], but over the narrower range in Fig. 5, a linear relationship is possible for the scattered data; the trend line in the figure has a r^2 value of 0.87. The low strain rate data for the Brock foams falls at the bottom of the scatter band for literature data [5], but the impact data

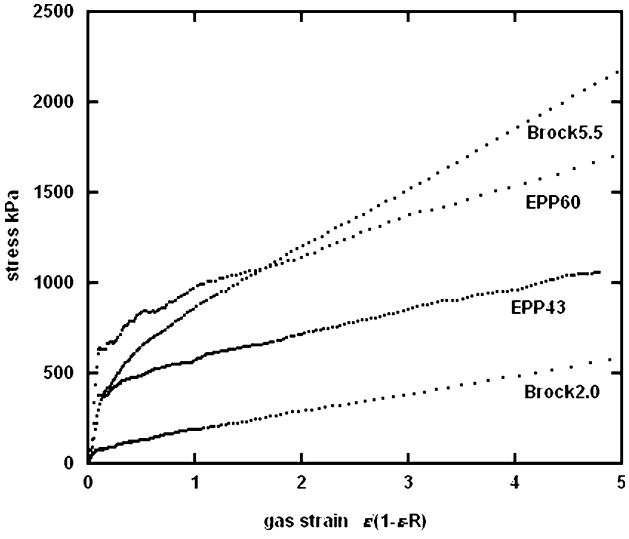

Fig. 4 Impact compressive stress–strain curves for four foams plotted according to Eq. 1. The straight-line fit parameters are given in Table 3

Table 3 Compressive impact tests at initial strain rate circa 200 s^{-1}

Foam	Relative density R	Initial yield stress σ_0(kPa)	Effective gas pressure p_0(kPa)
Brock FPP3.0	0.037	85 ± 5	103 ± 6
Brock FPP5.5	0.085	550	255 ± 5
BASF Neopolen 43	0.046	440 ± 5	135 ± 8
BASF Neopolen 60	0.066	760 ± 30	200 ± 10

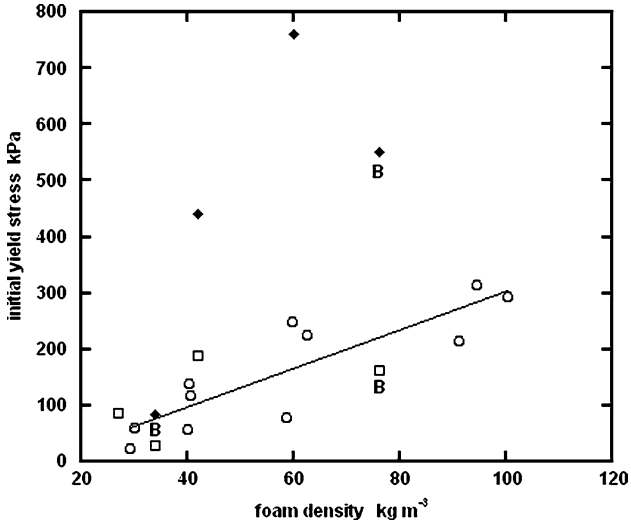

Fig. 5 Initial impact compressive yield stress (solid symbols) as a function of foam density compared with low strain rate data (open squares), and literature [5] (open circles) with trend line. B indicates Brock foam

Table 4 Compressive tests at initial strain rate 0.013 s^{-1}

Foam	Initial yield stress σ_0(kPa)	Effective gas pressure p_0(kPa)	Impact σ_0 / Instron σ_0
Brock FPP3.0	28 ± 1	75 ± 1	3.3
Brock FPP5.5	164 ± 3*	256 ± 3	3.4
BASF Neopolen 24	87 ± 2	107 ± 1	
BASF Neopolen 43	189 ± 2	131 ± 1	2.3

* Equation 1 was fitted using $R = 0.0$

for these foams is considerably lower than for the BASF EPP. Both the crystallinity of the PP and the microstructure of the Brock foams could differ from those of the BASF EPP. When the crystallinity of PP increases, both the tensile yield stress and the Young's modulus of the biaxially-oriented cell faces also increase.

Poisson's ratio

An Instron universal testing machine, fitted with a linear variable-displacement transducer (LVDT) to measure the compressive deflection, and a pair of LVDTs to measure the change in the foam block width, was used to measure Poisson's ratio both in the elastic and post-yield region. The surfaces of the metal plates, that applied the load, were covered with a polytetrafluorethylene (PTFE) coated glass-fibre cloth, to produce a low coefficient of friction surface. 12 mm high and 30 mm wide blocks of solid PTFE, attached to the ends of the spring loaded LVDT cores, pressed on the foam sides with a force of a few N. The initial sample height of 25 mm could be reduced to about 12 mm without the upper loading plate contacting the PTFE blocks. The cross-head speed was 20 mm min^{-1}, so the initial strain rate was 0.013 s^{-1}.

Figure 6 shows the lateral strain as a function of the compressive strain. The lateral strain remains within ±0.5% of zero for loading the EPP; on unloading there is a slight expansion, but the lateral strain increase is less than 0.3%. The behaviour of the Brock FPP3.0 foam (not shown) is similar to that of the EPPs.

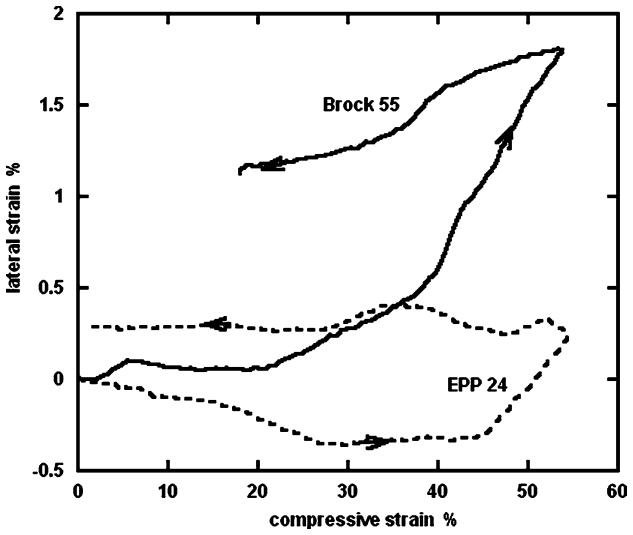

Fig. 6 Lateral strain as a function of the compressive strain for slow compression tests on two foams

However, for the Brock FPP5.5 foam of density 76 kg m^{-3}, after 20% compressive loading, there is a steady increase in the lateral strain, with values reaching nearly 2% at 55% compression. The initial phase, for strains <30%, probably occurs while beads come into contact in the direction of compression. The second phase, for strains between 40 and 60%, could be due to bead surfaces, in contact, shearing over each other, so pushing each other apart laterally. On unloading, there is strain recovery, but there is a residual lateral strain at zero load. The traces for the different foams are reproducible.

Plane strain indentation

The large channels between the Brock foam beads may affect the ease of indentation, compared with EPP. Consequently, *plane strain* indentation tests were performed in which the foam strains were confined to a single plane. The central part of a 25 by 100 mm side of a 25 by 25 by 100 mm block of foam was compressed by the lower horizontal surface of a 25 mm metal cube, while supported on a horizontal flat table on an Instron. The surfaces in contact with the foam were covered with PTFE coated cloth to minimise friction.

The mean indentation stress $\overline{\sigma}$ (the indentation force F divided by indenter lower surface area A) was compared with the stress σ_U to uniformly compress a block to the same nominal compressive strain ε (as in the Poisson's ratio experiment). The indentation stress ratio H is defined as

$$H \equiv \frac{\overline{\sigma}(\varepsilon)}{\sigma_U(\varepsilon)} \tag{2}$$

Figure 7 shows values of H as a function of compressive strain for the four foams. The values for the BASF EPP increase steadily to a maximum at 40 to 50% compressive strain. The strain variation of H is typical of open-cell polyurethane (PU) seating foams [14], but the peak H values for the PU foams are much larger at about 4. H reduces at high strains because the majority of the load is taken by the highly compressed foam between the indenter lower face and the support table. The H value for the Brock foams is a nearly constant, or slightly decreasing, function of strains between 10 and 50%. The lower values at 5% strain represent the elastic region.

A foam with a high resistance to indentation (a high H value) would be preferable to one with a low H value, for applications such as bicycle helmets. In a kerbstone impact test, the loading slope (impact force versus helmet deformation) is generally about half that

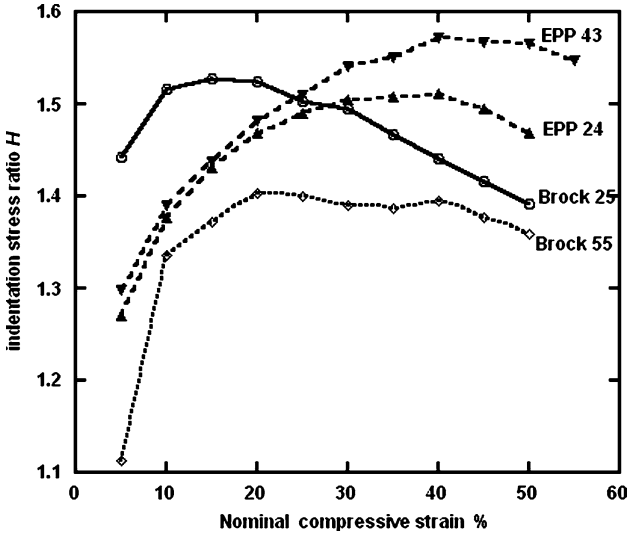

Fig. 7 Indentation stress ratio H as a function of compressive strain, for four foams

for an impact on a flat road surface [15] for helmet liners made of EPS. However the H values of the Brock foams are broadly comparable with those for the EPP foams, so there is unlikely to be any advantage of Brock foams in this application.

Water flow

Water flow was characterised with a simple rig, having a constant water head of $h = 130$ mm. A foam cylinder of length $L = 25.7$ mm and diameter 51.7 mm was attached to the end of a polypropylene tube. The curved surfaces of the foam were sealed with silicone sealant. Airflow characterisation was not attempted; these foams have such a large water permeability that the pressure gradient for airflow at 5 m s^{-1} is likely to be only a few kPa, hence difficult to measure accurately.

The pressure gradient (ΔP is the pressure drop across a foam length L) causing unidirectional, steady-state flow is related to the velocity of the medium V by

$$\frac{\Delta P}{L} = \frac{\eta}{K} V \tag{3}$$

where η is the medium viscosity (18×10^{-6} Pa s for air and 1.003×10^{-3} Pa s for water). The permeability K (m^2) is a material constant for airflow through uncompressed polyurethane foams.

The water permeability values were determined by measuring the water flow rate $\dot{m}$ in kg s^{-1}. Consequently, the foam permeability is given by

$$K = \frac{\eta \dot{m} L}{\rho^2 A g h} \tag{4}$$

where ρ is the density of water (998 kg m^{-3}), g is the acceleration of gravity and A is the cross-sectional area of the specimen. The values determined for Brock FPP3.0 and FPP5.5 foams respectively were 0.77×10^{-9} m^2 and 0.52×10^{-9} m^2.

Modelling

Foam structural models

The models were based on regular packing of uniform-sized beads on a body centre cubic (BCC) lattice. Such models are preferred over random structures because symmetry allows a small representative volume to be analysed. If random models are used, it is necessary to repeat the modelling many times, using a model containing perhaps 100 beads in a cubic box, to be able to estimate the average properties of the model. Although properties of the regular models are not as isotropic as those of the random models, they provide good estimates of the foam properties.

For airflow through open-cell polyurethane foams [8], the wet Kelvin foam model used is a good approximation of the foam geometry. Initially, for the bead foams, the inverse of the model was used. The starting point was a Kelvin open-cell foam having edges of constant, equilateral triangle cross-section; increasing the edge width increases the volume fraction of liquid V_A. *Surface Evolver* [16] software was then used to minimise the liquid/gas interface surface area. However, if V_A exceeds 0.11, the evolution process fails, with the square faces closing up. In the inverse model, the air locations are replaced by PP foam, and the solid PU locations by air. Therefore V_A becomes the volume fraction of air channels. This geometry also has a minimum surface area. Figure 8a shows the representative unit cell, for compression in the [001] direction, a triangular prism containing 1/16th parts of two spheres. The unit cell length is half of the lattice parameter d of the BCC lattice.

In EPP, EPS, or Brock foams, initially nearly-spherical beads contact and are pressed together. The pressure flattens areas where bead contact (the polymer is in the liquid state in EPS or EPP, and in the solid state in Brock foams). The shape of the 'free' part of bead surfaces probably does not change from being spherical. However, the inverse of the wet Kelvin model is still a reasonable approximation to the air

channel geometry of the bead foams when $V_A \leq 0.085$. The model of overlapping spherical beads on a BCC lattice, had been used previously for permeability computations [10]; it was used here with $V_A = 0.213$. Figure 8b shows the representative unit cell for the airflow calculations; the air channel is shaded while the beads are transparent. For a unit cell height of 1 mm, a sphere radius of 0.91416 mm produces the required V_A value. Note that the upper and lower surfaces contain a section of a single bead, whereas, in the wet Kelvin model, they contain sections of two beads.

The properties of both models are slightly anisotropic; the anisotropy of the wet Kelvin model is small, a factor of two for Young's modulus [17] and 1% for airflow permeability [8]. The [001] direction was chosen for the airflow direction or the compressive stress axis, since the representative unit cell is simpler than for the [111] direction.

Finite Element Analysis (FEA) of bead foam compression

The size of the representative unit cell for regular lattice models is much smaller than those in random models. Consequently, the former were used. The bead phase of the foam is taken to be a homogeneous material, with properties modelled by the *crushable foam* material model in ABAQUS version 6.5, while the air phase has zero mechanical moduli. The crushable foam model is for isotropic materials, which harden as the volume changes. The equation of the yield surface, which describes the stress states that cause yielding, is

$$\left(p - \frac{1}{2}(p_c - p_t)\right)^2 + \left(\frac{a\sigma_e}{b}\right) = a^2 \quad (5)$$

where σ_e is the von Mises equivalent stress, and p is the hydrostatic pressure component of the stress tensor. This yield surface, available as a material model in ABAQUS, had been successfully used [18] to describe yield data for polystyrene bead foam.

The section of the yield surface in the p σ_e plane is an ellipse, with half axes a and b in the p and σ_e directions respectively. The ellipse intercepts the p axis at $-p_t$ and p_{C0}, respectively the initial yield pressures in hydrostatic tension and compression. When the foam hardens, the ellipse increases in size, with the same axial ratio, with the coordinate p_t at the left remaining fixed, while that at the right moves to p_C. The parameters used in the *Crushable Foam* model are σ_{C0}/p_{C0} and p_t/p_{C0} followed by tabular hardening data for σ_C versus the true compressive strain ε_T.

It is not easy to select appropriate EPP data for modelling the Brock foams. Since they have a porosity $V_A = 0.25$, the bead density is 33% higher than the foam density, if the effect of the polyurethane adhesive on density is ignored. However, the Brock moulding process pre-crushes the regions where the beads contact, reducing the initial yield stress (this can be shown by repeated impact tests on EPP foam). Consequently, for the Brock foam of density 76 kg m^{-3}, the parameters were used from impact tests of EPP60:

(1) σ_{C0} measured at impact strain rates as 0.76 MPa.
(2) the previously used [14] $\sigma_{C0}/p_{C0} = 1.933$ was assumed to apply to the PP foam.
3) assuming $p_t = p_{C0}$, the initial yield pressure in hydrostatic tension $p_t = 0.76$ MPa.
4) tabulated data for σ_C versus the true compressive strain ε_T. σ_C was computed from Eq. 1, using the parameter for EPP60 in Table 3, at intervals of compressive true strain of 0.06. The first row of

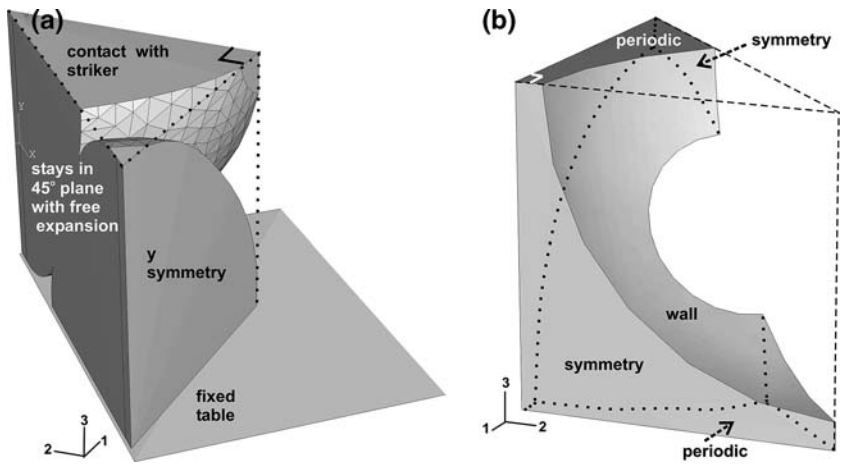

Fig. 8 Representative unit cells (dotted outline) for: (**a**) wet Kelvin model with $V_A = 0.085$, showing boundary conditions for FEA of the PP foam beads (shaded), (**b**) overlapping spherical beads with $V_A = 0.213$, showing boundary conditions for air flow in the channel (shaded)

this table is the initial yield stress σ_{C0} at zero true strain.

The compressive true strain is defined by

$$\varepsilon_T = -\ln \lambda \quad (6)$$

where λ is the extension ratio in the compression direction. For uniaxial compression, the Poisson's ratio in the post-yield regime is zero. Consequently $\varepsilon_($ is also equal to the true volume strain. Prior to yield the foam is assumed to be elastic, with a Young's modulus estimated as 6.0 MPa [5], and a Poisson's ratio of 0.1.

When the Standard (Implicit) form of ABAQUS was used to model the Brock foams, the simulation was only stable to low compressive strains. Elements turned inside out near high stress regions, such as the 'crack' where two beads join. To make useful predictions of the foam compressive stress–strain curve, the FEA should proceed to compressive strains >0.6. Consequently, the Dynamic (Explicit) form of ABAQUS was used; this calculates forces, then predicts the accelerations of element masses to find their position in the next time step. The wet Kelvin model was used with an edge width of 0.35, corresponding to $V_A = 0.085$, and the overlapping sphere model with $V_A = 0.213$.

A material damping factor $\alpha = 0$ was used for the PP foam. The general contact condition was used for foam contact, either with other foam surfaces, the support table or the striker face, with a negligibly small friction coefficient of 0.001. The pressure versus over-closure relationship used was non-linear, with linear interpolation between over-closures (at pressures in MPa) of 0 (1), 3 μm (0.2), 6 μm (1.0), 10 μm (5), and 15 μm (100). Such a relationship, while necessary to keep the time interval reasonably large, has little effect on the predicted foam response.

The part was seeded with 14 seeds along a bead radius, then meshed with modified 10-node quadratic tetrahedral elements (C3D10M), of which there were typically 11,700; Fig. 10a shows the mesh on the bead surfaces. For a run to compute the volume of the deformed model, linear elements had to be used, since the element volume parameter EVOL produces nonsense when quadratic elements are used. Although the BCC lattice parameter was taken as 1.0 mm, the value does not affect the predicted stress–strain curve. The representative unit cell lower surface was constrained to be in contact with a lower fixed rigid plate (Fig. 8a). On the unit cell side faces that lie in the 13 and 23 planes, the boundary conditions are of y and x symmetry respectively. On the side face at 45° to these faces, no rotations are allowed that would take the polymer surface out of the plane, and a constraint of constant displacement normal to the plane, means that this plane can expand freely.

The impacting plate of 1 kg mass has a horizontal (in the 12 plane) flat lower face, and a single degree of freedom to move in the 3 direction. Its initial velocity of 1 m s^{-1} is not significantly reduced during the impact, so the foam strain increases linearly with time.

FEA predictions of foam compression

The FEA, of a BCC array of beads of uniform size, predicted 'average stress' versus 'average strain' curves for the compressive impact of the foams (Fig. 9a). That for the wet Kelvin model with $V_A = 0.007$ is almost identical to one predicted for impact compression of a prism of solid foam, showing that the small volume of air channel has negligible effect. In that for the model with $V_A = 0.085$ the initial yield point is less marked, and the stress is reduced somewhat. In that for the overlapping spheres model with $V_A = 0.213$, the stress–strain curve becomes almost linear. However, this does not indicate an elastic response. As V_A rises, the linear region extends to a higher compressive strain. Figure 9a shows that the volume fraction of the deformed model occupied by inter-bead channels reduces progressively with increasing compressive strain. However, in spite of parts of the channels closing, the volume fraction of channel does not become zero.

Figure 9b gives the impact compressive stress–strain data for two foams. The EPP60 graph has a near identical shape to the predictions for the solid foam in Fig. 9a; the difference is due to the approximation of fitting the experimental data with Eq. 1. The Brock FPP5.5 graph is almost as linear as the prediction for $V_A = 0.213$ in Fig. 9a, but there is still an initial yield bump at a strain of 0.1.

In the $V_A = 0.213$ model, some beads are initially separated by a gap in the direction of applied stress (Fig. 10a); these approach and touch as the compressive strain increases. Contour maps (Fig. 10b, c) show that the vertical compressive stress is non-uniform in the foam, with very low values near the bead free surfaces in the corner of the unit cell. The foam is predicted to start yielding near the 'crack tips' on the 45° plane (shown in Fig. 8a) for compressive strains exceeding 5%. Therefore, the foam density increases progressively, but non-uniformly, as the mean foam compressive strain increases.

The FEA predicted the lateral expansion strain of the representative unit cell (Fig. 11). For all the models, the behaviour up to a compressive strain of

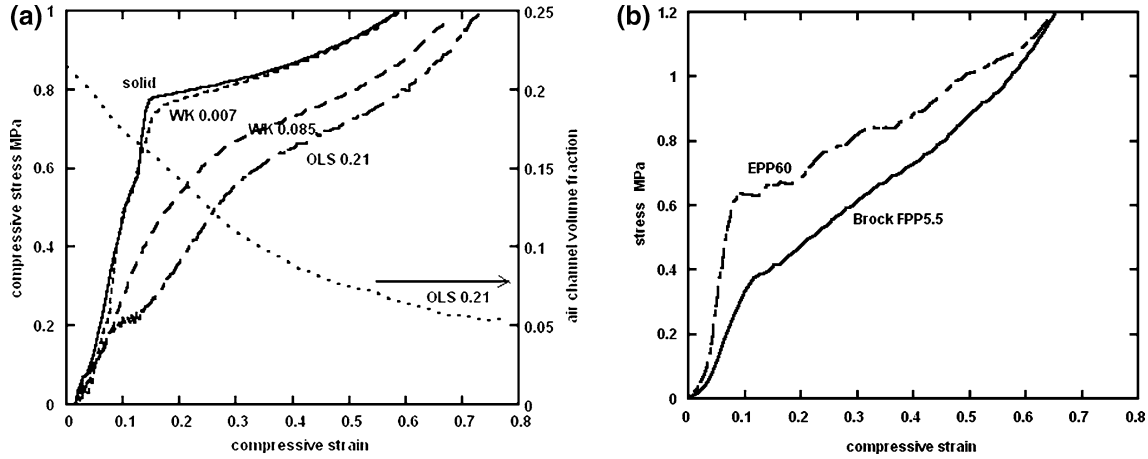

Fig. 9 Impact compressive stress versus strain: (**a**) predicted by FEA for solid EPP60 and three bead-foam models with V_A values, (**b**) experimental data for the Brock FPP5.5 and BASF PP60 foams. The variation of air channel volume fraction is also shown in Fig. 9a for the overlapping sphere model

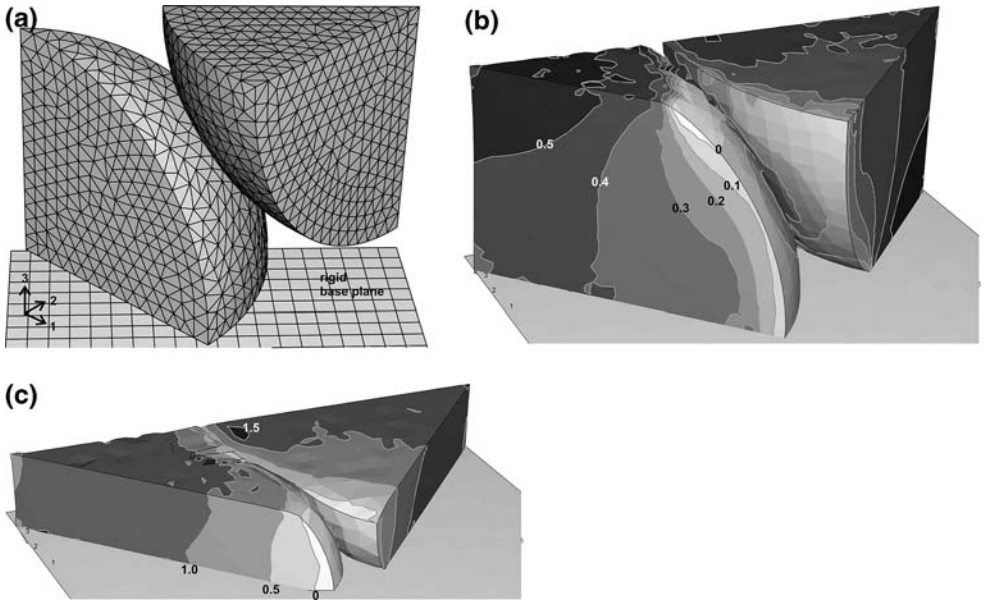

Fig. 10 FEA of the overlapping sphere model with $V_A = 0.213$: (**a**) undeformed showing mesh, (**b**) and (**c**) deformed, with contours of compressive stress σ_{33} in MPa at average strains of (b) 40%, (c) 80%

0.15 corresponds to a Poisson ratio of 0.1. For the higher V_A models, sliding of the touching bead surfaces, oblique to the compressive stress direction, causes further lateral expansion, then the lateral strain becomes constant at about 3%. The post-yield lateral strains are predicted to increase more slowly for the $V_A = 0.007$ model. For compressive strains <20%, the predicted lateral strains increase rapidly, whereas the experimental strains remain near zero. However, at a 50% compressive strain the predicted lateral strain for the overlapping sphere model is only about twice that measured for the Brock 5.5 foam. The effect of increasing V_A (from the EPP 24 to the Brock FPP5.5 foam) on the lateral expansion is correctly predicted.

Computational Fluid Dynamics (CFD)

CFD method

CFD can predict air or water flow through channels of complex geometry. The CFD program Fluent 6 [19] was used. The geometries of the representative unit cells, for the wet Kelvin or overlapping sphere models, were imported into the pre-processor Gambit. This allowed the boundaries to be assigned as *wall* (for the curved channel walls), *symmetry* (for the flat midplanes of channels which lie either in the 13 or 23 planes), or *periodic* (for the identical sized, parallel entry and exit surfaces) as shown in Fig. 8b. The model could be

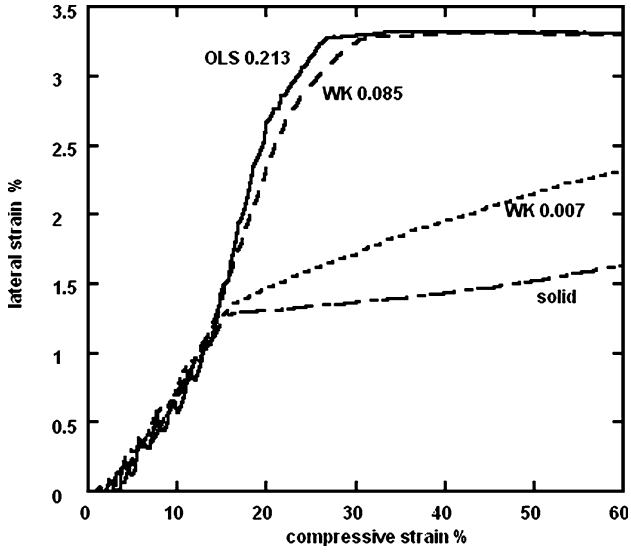

Fig. 11 FEA predicted lateral expansion strain versus compressive strain, for three models, with V_A values shown

scaled to analyse the effect of bead size. The channel was meshed with tetrahedra, and the mesh exported for use in Fluent. For the wet Kelvin foam model with a unit cell length of 0.5 mm, the tetrahedron edge length was 10 μm, producing between 15,000 and 27,000 elements. Gambit could only satisfactorily mesh the overlapping sphere model with spherical surfaces when the tetrahedron edge length was 130 μm; consequently a single element spanned the narrowest part of the channel, and there were only 393 elements. To allow a refined mesh, the shape was imported into the Computer Aided Drawing package Rhino, meshed with triangles, and the mesh converted back into a geometrical object having facetted, curved surfaces. It was then possible to mesh this object in Gambit with a tetrahedron edge length of 25 μm, producing 13,100 elements in a double-length unit cell.

Analyses were made for laminar, isothermal airflow in the [001] direction under a pressure gradient of 100 Pa m^{-1}, for wet Kelvin and overlapping sphere models. The discretization for momentum used the *second order upwind* scheme for successive approximations of the flow field, with under-relaxation factors of 0.2 for pressure, 0.4 for momentum, 1 for body forces and 1 for density. Iteration was continued until the velocity changes at all grid points were less than 10^{-9} m s^{-1} and the flow output converged to a constant value. Checks were made that refinement of the mesh did not change the predicted air permeability by more than 1%.

The flow rate Q was computed, as the surface integral of the z velocity component on the periodic boundary. The mean air velocity $\overline{V}$ in the foam is Q divided by the cross sectional area of the prismatic unit. It is substituted in Eq. 1 to compute the foam permeability

$$K = \eta \bar{V} \Big/ \frac{\Delta P}{L} \tag{7}$$

CFD predictions

The predicted air velocity field in the channels between the beads in the overlapping sphere model with $V_A = 0.213$ is shown in Fig. 12a. The velocities are, as expected, greatest in the centre of the straight 'open' channel through the lattice in the [001] direction, and low in regions where spheres nearly touch along [001]. The maximum velocity was 0.127 m s^{-1} for this simulation. In the wet Kelvin models, there is no open channel along the lattice [001] direction; consequently the maximum airflow velocities occur in the narrow 'throats' of the channels that run at 45° to the [001] direction (Fig. 12b); the maximum velocity was 0.00213 m s^{-1}. The foam permeability K was calculated using Eq. 7 and the cross sectional area of the model. Table 5 shows that, for a fixed lattice parameter d, K initially increases slightly faster than the square of V_A then suddenly increases further when straight open channels develop along the [001] direction.

Larson and Higdon [10] used a boundary collocation method to analyse Stokes flow in the overlapping sphere model. They normalised their results by dividing the permeability by the square of the BCC lattice spacing d, since K scales with d^2 for periodic cubic models. The CFD results in Table 5 confirm this scaling. Their results for the normalised permeability as a function of the model air volume fraction are compared in Fig. 13 with the CFD result for the overlapping sphere model; their predictions, using a completely different analytical method, validate the CFD prediction for the overlapping sphere model. Their predictions fit the power law relationship

$$\frac{K}{d^2} = 7.51 \times 10^{-3} V_A^{2..62} \tag{8}$$

with a correlation coefficient $r^2 = 0.9999$. The CFD predictions for the wet Kelvin model fall slightly below their data, as expected. Using Eq. 8 with mean bead diameter $d = 4.6$ mm for the FPP3.0 foam and 3.1 mm for the FPP5.5 foam, and a porosity $V_A = 0.25$, predicted permeabilities of 4.2×10^{-9} m^2 and 1.9×10^{-9} m^2 respectively. Thus the measured Brock

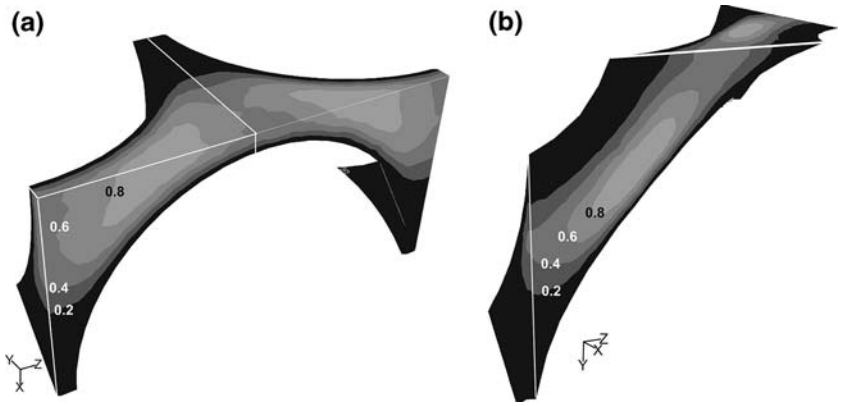

Fig. 12 Perspective view of the CFD predicted air velocity contours of: (a) overlapping sphere model with $V_A = 0.213$, (b) wet Kelvin model with $V_A = 0.062$. The contours, at 20% intervals of the maximum velocity, are shown on the symmetry and input planes of the channels between the beads

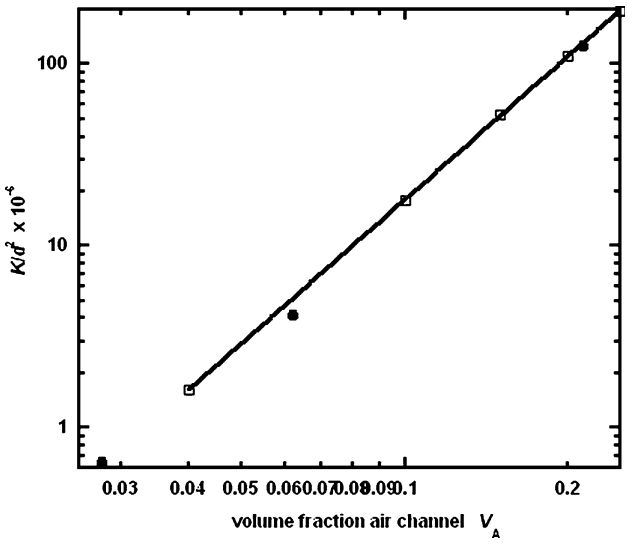

Fig. 13 Normalised foam air permeability versus volume fraction air channels: solid data points CFD results. The trend line fits open data points from Larson and Higdon [10]

foam permeabilities are respectively 18% and 27% of the predicted values.

Discussion

The predicted compressive response of a wet Kelvin bead foam with $V_A = 0.007$ is close to that of the homogeneous material. Therefore the treatment of EPS and EPP as homogeneous materials is reasonable, and there is no need to revise the mechanics analysis of these materials. The air or steam permeability, although very low, is sufficient to accelerate the cooling phase of the bead moulding process.

The Brock foams have novel properties due to their higher volume fraction of inter-bead channels. The patent [11] and promotional material say that, on (localised) impact, compressive forces radiate outwards to surrounding beads. The beads are said to try to separate from adjacent beads sideways, deflecting energy away from the body. This *force radiation* concept, if it means load spreading from a localised indentation, also applies to conventional EPP foam; the indentation H values for the two types of foam were similar. The successful FEA modelling, of how the compressive stress–strain response and lateral expansion of Brock-type foam relates to that of EPP foam of much lower channel porosity, invokes conventional foam mechanics. It is not necessary to invoke a (physically unrealistic) mechanism of stress radiating in all directions. Although the Brock foam contains a range of bead sizes, and the packing is random, the use of a model with a regular array of uniform-sized beads does not introduce a significant error; foam compressive properties average the response of a large number of beads, and the volume fraction of air channel determines the response.

Table 5 Airflow predictions for a pressure gradient of 100 Pa m^{-1}

Model & channel edge width	Air volume fraction V_A	Lattice d(mm)	Air flow Q(m^3 s^{-1})	Permeability K(m^2)	K/V_a^2 $\times 10^{-9}$ (m^2)	K/d^2 $\times 10^{-6}$
Kelvin 0.2	0.0276	1.0	4.495×10^{-13}	6.47×10^{-13}	0.849	0.647
Kelvin 0.3	0.0622	1.0	2.899×10^{-12}	4.17×10^{-12}	1.078	4.17
Touching spheres	0.2131	1.0	8.815×10^{-11}	1.269×10^{-10}	2.79	127
		2.0	1.410×10^{-9}	5.075×10^{-10}		127
		4.0	2.234×10^{-8}	2.010×10^{-9}		126

The lateral expansion of compressed Brock foam, while greater than that of EPP, is not very large. The FEA models, based on [001] direction compression of a BCC lattice of beads, predict too high a lateral strain. This is not surprising, since the Kelvin model for polyurethane open-cell foam [20] predicts too high a Poisson's ratio for compression in the [001] direction; a result of the chains of square faces, linked corner to corner, that run in this direction. In the random-packed bead structure of the Brock and EPP foams, there is no similar mechanism to increase the lateral strain. It is possible that the modelling could be improved by using a larger Young's modulus for the foam beads, and a higher coefficient of friction for bead-to-bead contact.

The compressive properties of a block of Brock foam, considered as a structure, can be compared with that of truncated pyramids of EPS packaging [18]. The macroscopic geometry of the packaging pyramid, and the microscopic geometry of the bonded-bead foam, cause the force-deflection curve to be almost linear.

The impact energy absorbed by unit volume of foam is equal to the area under the compressive stress–strain graph. The maximum stress on this graph can, for some applications, be set by an injury criterion. The foam density can be chosen so the initial yield stress and hardening suit the application. If the energy absorption efficiency, defined as the area under the compressive stress–strain curve (up to a particular stress) divided by the stress [21], is calculated for the Brock foams, it will be slightly lower that the circa 0.4 value for EPP for stresses between 0.1 and 1 MPa. The Brock foams have a more linear compressive stress–strain curve than EPP foams of similar density, so have a disadvantage in terms of energy absorption efficiency. Foam with a constant compressive stress would have an efficiency of 1 if that stress could be tolerated by the application.

The measured water permeabilities of the Brock foams are between 20 and 30% of the values predicted by models containing uniform-sized beads. The range of bead sizes in the real foam, and the use of polyurethane adhesive, probably reduce the mean channel diameter, hence the permeability. Hence, the regular lattice model for permeability is not ideal. The predictions for the Brock foams contrast with those for open-cell polyurethane foams, where the measured air permeabilities were larger than the predicted values [8]. The two types of foam, with completely different porosity, have permeabilities of the same order of magnitude, since the cells in the open cell foam are much smaller than the beads in the bonded-bead foam.

The predicted permeability of the overlapping sphere model foam agrees with earlier predictions [10] for this model, varying with close to the 2.6th power of porosity and with the square of bead size. Hence, if the beads can be made sufficiently large and the porosity increased, the permeability can be made quite large. However, such a foam would be mechanically weak. The water permeability of foam is of interest in applications such as cushioning under artificial sports surfaces, which are watered.

The Brock foam permeability is unlikely to be sufficient for it to be used as the liner of a bicycle helmet without ventilation holes. Bicycle helmets require an external microshell to provide the tensile strength which EPS lacks, and to minimise surface indentation in impacts. Current microshells are impermeable, so would prevent airflow through Brock foam. For this reason, and because of the low energy absorption efficiency, Brock foams are not ideal for use in bicycle helmets.

A similar type of bead-level modelling could usefully be applied to the fracture toughness of polymeric bead foams; that of EPS is known to be very low. It would also be of interest to model randomly packed beads, with a size distribution, to improve the prediction of permeability. However, this would be a significant computational challenge. A framework has been established for designing porous energy-absorbing products, based on the random packing of beads. There is found to be a trade off between increased permeability and decreased energy absorption per unit volume, in these isotropic materials. However, this relationship does not apply to anisotropic products containing a few large channels in particular directions, which maximise the airflow through the product.

Acknowledgment The authors thank EPSRC for support under Grant R89790, and both Brock USA and BASF for providing foams.

References

1. Svec P, Rosik L, Horak Z (1990) Styrene based plastics and their modification. Ellis Horwood, London
2. Skinner SJ, Baxter S, Eagleton SD, (1965) Plast Eng 42:171
3. Mills NJ (1997) Cell Polym 16:194
4. Beverte I (2004) J Cell Plast 40:191
5. Ibba A, Avalle M (2003) Identificazione di schiume in polipropilene e relazione tra densita e parametric dei modelli, www.pcm.unifi.it/lavorasalerno/ART_056.pdf (AIAS Congress, Salerno)
6. Zohdi TI (2003) Proc Roy Soc 459A:1395
7. Mills NJ (2004) *Polyolefin foams*, RAPRA review report 167 (vol 14, no 11) ISBN 1-85957-434-3, 136 pp
8. Mills NJ (2005) J Mater Sci 40:5845
9. Hill RG, Koch DL, Ladd AJC (2001) J Fluid Mech 448:243
10. Larson RE, Higdon JJL (1988) Phys Fluids A1:38

11. Bainbridge DW, Nickerson LP, Denton GC (2002) US Patent 6,453,477 Protective padding for sports gear
12. Mills NJ (1994) In: Hilyard NC, Cunningham A (eds) Low density cellular plastics, Chapman & Hall, 270–318
13. Mills NJ (2005) Plastics: microstructure and engineering applications, 3rd edn Butterworth Heinemann, p 126
14. Mills NJ, Gilchrist A (2000) Cell Polymer 19:389
15. Mills NJ, Gilchrist A (2005) Dynamic FEA of bicycle helmet oblique impact, submitted to Int J Impact Eng
16. Surface Evolver (2004) at //www.susqu.edu/facstaff/b/brakke/evolver/
17. Mills NJ (2007) Int J Solids Struct 44:51
18. Masso-Moreu Y, Mills NJ (2003) Int J Impact Eng 28:653
19. *Fluent Manual*, Fluent Inc, Lebanon, USA
20. Zhu H, Mills NJ, Knott JF (1997) J Mech Phys Solids 45:1875
21. Avalle M, Belingardi G, Montanini R (2001) Int J Impact Eng 25:455